

## EFFECT OF STOICHIOMETRY AND STRAIN RATE ON TRANSIENT FLAME RESPONSE

OMAR M. KNIO<sup>1</sup> AND HABIB N. NAJM<sup>2</sup>

<sup>1</sup>*Department of Mechanical Engineering  
Johns Hopkins University  
Baltimore, MD 21218-2686, USA*

<sup>2</sup>*Combustion Research Facility, MS 9051  
Sandia National Laboratories  
Livermore, CA, 94550, USA*

The interaction of a premixed methane/air flame with a counter-rotating vortex pair is analyzed using a parallel low-Mach-number computational model that is based on a detailed  $C_1C_2$  chemical mechanism. Attention is focused on the transient response of the heat release rate and the flame structure at the centerline of the vortex pair. Results are obtained for vortex pairs of different strengths under lean, stoichiometric, and rich conditions. For the range of vortex strengths considered, the computations indicate that the heat release rate in the rich flame decays significantly faster than in the stoichiometric flame; this behavior is consistent with recent experimental measurements. Meanwhile, the heat release rate in the lean flame decays at a slightly slower rate than in the stoichiometric flame. The transient response of flame radicals such as H, CH, OH, and HCO is also analyzed. The analysis reveals a complex nonlinear dependence of the transient structure on both the vortex strength and the stoichiometry.

### Introduction

Unsteady interactions of premixed flames with vortical structures are an essential feature of many reacting flow applications, including burners, combustors, furnaces, and fires. Consequently, numerous efforts have focused on isolating these interactions and on analyzing flame response to unsteady strain.

One common approach to addressing this issue is based on one-dimensional studies of opposed jet flames with imposed sinusoidal perturbations [1–3]. These studies have established a number of interesting trends, in particular concerning the effects of imposed strain amplitude and frequency and of the mixture stoichiometry. Dynamic features have also been identified, including extinction, partial extinction, and reignition.

A second approach is based on analyzing flame interactions with vortices [4–6], counter-rotating vortex pairs [7–11], or toroidal vortex rings [12–14]. These investigations have also led to several observations regarding unsteady heat release and have in addition enabled the study of multidimensional phenomena, including flame stretch and contortion, pocket formation, and baroclinic vorticity generation.

There appears to be a strong similarity between the one-dimensional strained flame and the *local* flame zone at the centerline of a counter-rotating vortex pair. In both situations, the flame is subjected

to an unsteady strain field, while curvature effects are naturally minimized. Consequently, one may be inclined to expect a similar flame response, at least in a qualitative fashion. However, this similarity may not necessarily hold. A specific example was provided in our recent effort [15], which focused on the interaction of rich and stoichiometric flames with a counter-rotating vortex pair. Consistent with experimental results, the computations in Ref. [15] found that the rich flame exhibits a faster response to the unsteady strain than the stoichiometric flame. This behavior is in contrast to the opposed-jet flame study in Ref. [2], which noted that the sinusoidally excited rich flame has a slower response than the stoichiometric flame.

The above results raise a variety of questions regarding the origin of the observed differences between the strained one-dimensional flame results and the strained flame at the centerline of the vortex pair. One possible cause behind these differences concerns the imposed strain, whose large values in the two-dimensional flow may prevent us from using a linearized analysis to establish a relationship with the one-dimensional flame under sinusoidal perturbations. Another possibility concerns the flame configuration itself, which is typically anchored in the one-dimensional setting and freely propagating in the two-dimensional case.

Motivated by the desire to resolve and reconcile these differences, the present work focuses on the

Report Documentation Page				Form Approved OMB No. 0704-0188	
Public reporting burden for the collection of information is estimated to average 1 hour per response, including the time for reviewing instructions, searching existing data sources, gathering and maintaining the data needed, and completing and reviewing the collection of information. Send comments regarding this burden estimate or any other aspect of this collection of information, including suggestions for reducing this burden, to Washington Headquarters Services, Directorate for Information Operations and Reports, 1215 Jefferson Davis Highway, Suite 1204, Arlington VA 22202-4302. Respondents should be aware that notwithstanding any other provision of law, no person shall be subject to a penalty for failing to comply with a collection of information if it does not display a currently valid OMB control number.					
1. REPORT DATE <b>04 AUG 2000</b>		2. REPORT TYPE <b>N/A</b>		3. DATES COVERED <b>-</b>	
4. TITLE AND SUBTITLE <b>Effect of Stoichiometry and Strain Rate on Transient Flame Response</b>				5a. CONTRACT NUMBER	
				5b. GRANT NUMBER	
				5c. PROGRAM ELEMENT NUMBER	
6. AUTHOR(S)				5d. PROJECT NUMBER	
				5e. TASK NUMBER	
				5f. WORK UNIT NUMBER	
7. PERFORMING ORGANIZATION NAME(S) AND ADDRESS(ES) <b>Department of Mechanical Engineering Johns Hopkins University Baltimore, MD 21218-2686, USA</b>				8. PERFORMING ORGANIZATION REPORT NUMBER	
9. SPONSORING/MONITORING AGENCY NAME(S) AND ADDRESS(ES)				10. SPONSOR/MONITOR'S ACRONYM(S)	
				11. SPONSOR/MONITOR'S REPORT NUMBER(S)	
12. DISTRIBUTION/AVAILABILITY STATEMENT <b>Approved for public release, distribution unlimited</b>					
13. SUPPLEMENTARY NOTES <b>See also ADM001790, Proceedings of the Combustion Institute, Volume 28. Held in Edinburgh, Scotland on 30 July-4 August 2000.</b>					
14. ABSTRACT					
15. SUBJECT TERMS					
16. SECURITY CLASSIFICATION OF:			17. LIMITATION OF ABSTRACT <b>UU</b>	18. NUMBER OF PAGES <b>7</b>	19a. NAME OF RESPONSIBLE PERSON
a. REPORT <b>unclassified</b>	b. ABSTRACT <b>unclassified</b>	c. THIS PAGE <b>unclassified</b>			

effects of strain amplitude on the interaction between a premixed methane/air flame and a counter-rotating vortex pair. Parallel computations are performed using a two-dimensional, low-Mach-number reacting flow model that is based on a detailed C<sub>1</sub>–C<sub>2</sub> chemical mechanism. As further discussed below, we consider vortex pairs of different strengths, and in each case results are obtained at stoichiometric ( $\Phi = 1$ ), rich ( $\Phi = 1.2$ ), and lean ( $\Phi = 0.8$ ) conditions. The flame response is analyzed by contrasting the transient evolution of the heat release rate as well as flame radicals, including CH, OH, H, and HCO. These detailed computations are made possible using recent algorithmic developments, which are highlighted in the following section.

### Formulation and Numerical Schemes

The computational model used in the simulations below is adapted from our previous efforts in Refs. [16,17], which provide a detailed discussion of the numerical construction. Brief descriptions of the physical formulation and numerical scheme are provided below.

#### Physical Model

The physical model is based on the zero-Mach-number, compressible flow approach [18] which ignores acoustic waves and allows us to decompose the pressure into a spatially uniform component  $P_0(t)$  and a hydrodynamic component  $p(\mathbf{x}, t)$  which varies both in space and time. We assume a two-dimensional open domain, a gas mixture with zero bulk viscosity, and a detailed chemical kinetic mechanism involving  $N$  species and  $K$  elementary reactions. Sorret and Dufour effects are ignored, as are body forces and radiant heat transfer. The mixture is also assumed to obey the perfect gas law, with individual species molecular weights, specific heats, and enthalpies of formation.

Under the above assumptions, the governing equations are expressed in non-dimensional form as [16,17]

$$\begin{aligned} \frac{\partial \rho}{\partial t} = & \rho \left( -\frac{1}{T} \left[ -\mathbf{v} \cdot \nabla T + \frac{1}{RePr} \frac{\nabla \cdot (\lambda \nabla T)}{\rho c_p} \right. \right. \\ & + \left. \frac{1}{ReSc} \frac{\mathbf{G} \cdot \nabla T}{\rho c_p} + Da \frac{w_T}{\rho c_p} \right] \\ & \left. - \bar{W} \sum_{i=1}^N \frac{1}{W_i} \frac{\partial Y_i}{\partial t} \right) \end{aligned} \quad (1)$$

$$\frac{\partial(\rho u)}{\partial t} + \frac{\partial(\rho u^2)}{\partial x} + \frac{\partial(\rho uv)}{\partial y} = -\frac{\partial p}{\partial x} + \frac{1}{Re} \Phi_x \quad (2)$$

$$\frac{\partial(\rho v)}{\partial t} + \frac{\partial(\rho vu)}{\partial x} + \frac{\partial(\rho v^2)}{\partial y} = -\frac{\partial p}{\partial y} + \frac{1}{Re} \Phi_y \quad (3)$$

$$T = P_0 \bar{W} / \rho \quad (4)$$

$$\frac{\partial(\rho Y_i)}{\partial t} = -\nabla \cdot (\rho \mathbf{v} Y_i) + \frac{1}{ReSc} \nabla \cdot \mathbf{g}_i + Daw_i \quad (5)$$

respectively. Here,  $\rho$  is the density;  $T$  is the temperature;  $\mathbf{v} = (u, v)$  is the velocity vector;  $Y_i$  is the mass fraction of species  $i$ ;  $\mu$  is the dynamic viscosity;  $\lambda$  is the thermal conductivity;  $c_p$  is the mixture specific heat;  $\mathbf{g}_i$  is the diffusive mass flux of species  $i$ ;

$$\mathbf{G} \equiv \sum_{i=1}^N c_{p,i} \mathbf{g}_i$$

$c_{p,i}$  is the specific heat of species  $i$ ;  $W_i$  and  $w_i$  are the molecular weight and chemical production rate of species  $i$ , respectively;

$$\bar{W} \equiv 1 / \left( \sum_{i=1}^N Y_i / W_i \right)$$

$w_T$  is the rate of chemical heat release;  $Re$ ,  $Pr$ ,  $Sc$ , and  $Da$  are the Reynolds, Prandtl, Schmidt, and Damköhler numbers, respectively; and  $\Phi_x$  and  $\Phi_y$  are the viscous stress terms. For computational efficiency, and given that the flow cases under study involve significant N<sub>2</sub> dilution, mixture transport properties are set to those of N<sub>2</sub>, and species diffusion coefficients are set to those into N<sub>2</sub> at the local temperature.

#### Numerical Scheme

Numerical simulation of the governing equations is performed using a stiff, operator-split, finite-difference scheme whose construction is detailed in Ref. [17]. The scheme is a variable-density projection method for reacting flow, which relies on a second-order spatial discretization of the governing equations. Field variables are discretized using a staggered grid with uniform cell size along each coordinate direction. Velocity components are specified at cell edges, while scalar variables are specified at cell centers.

One of the key features of the computational construction in Ref. [17] is the use of a symmetric splitting of the diffusion and reaction terms and the incorporation of a stiff scheme for the numerical integration of the reaction source term. The splitting is implemented in such a way that the diffusion terms are updated in two half-time-step integrations, which are separated by a full-time-step integration of the reaction terms. Each diffusion half-step comprises several fractional substeps, which allows the use of a global time step that is several times larger than the critical diffusional time step. Meanwhile, the reaction source terms in the species and density equations are handled using a stiff integrator, which is adapted from the DVODE package [19].

The convergence properties and computational performance of the stiff, split scheme are also discussed in Ref. [17]. In particular, tests demonstrate that the construction is effective in defeating the stiffness of both the diffusion and reaction source terms. This leads to order-of-magnitude speedup over explicit, non-stiff schemes and enables large-scale unsteady computations of reacting flow with detailed kinetics.

## Results and Discussion

Computations of the interaction of a premixed methane/air flame with a two-dimensional vortex pair are performed in a rectangular,  $0.4 \times 1.6$  cm domain. The domain is discretized using a uniform grid with  $256 \times 1024$  cells and mesh size  $h = 15.625 \mu\text{m}$ . This fine resolution level is needed to adequately resolve the flame structure. The initial condition consists of the superposition of the velocity field induced by a periodic row of vortex pairs, with temperature, density, and mass fraction distributions of a steady-propagating, one-dimensional premixed flame computed with CHEMKIN [20,21]. We use the GRIMech 1.2 [22] mechanism with 32 species and 177 reactions. The flame is initially flat and horizontal, with reactants below and products on top. The vortex pair, initially in the reactants, propagates upward into the flame.

We consider  $\text{N}_2$ -diluted methane/air reactants mixtures with varying stoichiometry. Included in the analysis are lean ( $\Phi = 0.8$ ), rich ( $\Phi = 1.2$ ), and stoichiometric mixtures. In all cases, a 20%  $\text{N}_2$  dilution level is used. In addition to the stoichiometry, we vary the initial characteristics of the vortex pairs. In all cases, the initial distances between the vortex centers in a pair is held fixed,  $\delta = 0.25$  cm. On the other hand, the strengths of the vortices are varied by up to a factor of 10; we use  $\Gamma = 0.07, 0.028$ , and  $0.007 \text{ m}^2/\text{s}$ . Since the self-induced velocity of the vortex pair is proportional to its strength, these cases are referred to as fast, moderate, and slow, and labeled F, M, and S, respectively. As will be shown later, the peak strain rate field experienced by the flame also scales proportionally with the vortex strength.

### Flame–Vortex Interaction

In all cases, simulations are carried over a 0.5 ms period in order to observe the transient flame response to the strain rate field induced by the vortex pairs. Fig. 1 shows the heat release rate and vorticity fields at the end of the computations for all nine cases. The interaction between the flame and the vortex pair leads to the generation of opposite sign vorticity [4,10], which is depicted in Fig. 1 using dashed contours. Note that identical contour (vorticity) and shading (temperature) levels are selected

in all frames. As the strength of the vortex pair is increased, the number of vorticity contours increases; the vortex penetration distance into the flame and the extent of flame stretching increase as well. Note that in case S, the interaction is still in its early stages, flame deformation is weak, and a robust flame region is observed at all values of  $\Phi$ . For case F, however, significant contortion of the flame occurs, and it is evident from Figure 1 that the peak heat release rate in the rich flame has dropped significantly. This indicates that flame response depends substantially on both the vortex strength and the stoichiometry.

### Unsteady Strain Rate

In order to analyze these changes, we first quantify the unsteady strain rate that the flame experiences during the interaction. We focus our attention on the centerline of the vortex pair, where the stretching of the flame is large and the curvature of the front is small. We choose the location of  $10\% Y_{\text{fuel,max}}$  as a reference flame location, where the tangential strain rate is computed. The results, plotted in Fig. 2, indicate that the flame is subjected to strain rates that increase in proportion to increased vortex circulation in cases S, M, and F. For a given initial vortex strength, the strain rates vary with time and stoichiometry. This is most accentuated in the F cases, where significant flame contortion and baroclinic vorticity generation occur (see Fig. 1). In these cases, the strain rates in the lean and rich flames are higher than in the stoichiometric flame. Results suggest that this development is a consequence of the flame interaction with the flow. Baroclinic vorticity generation at the flame leads to the formation of a vortex dipole in the vicinity of the primary vortex [4,10]. The results suggest that the strength of the opposite-sign vortex dipole and its position during the interaction result in the observed difference in the strain rate levels.

On the other hand, the variations of strain with time and stoichiometry are relatively weak and fall within  $\pm 10\%$  of the mean. This provides a reasonable basis for examining the effect of stoichiometry on the transient flame response, as the strain rate is roughly the same for the three stoichiometries in each of the F, M, and S cases.

### Heat Release

The global flame response is interpreted in terms of the peak heat release rate, whose evolution is plotted in Fig. 3. The profiles are normalized by their initial values in each case. The results indicate that the peak heat release rate decays as the vortex pair impinges into the flame. Consistent with the trend in the strain rates, the rate of decay in heat release is faster as the vortex strength increases. Fig. 3 also

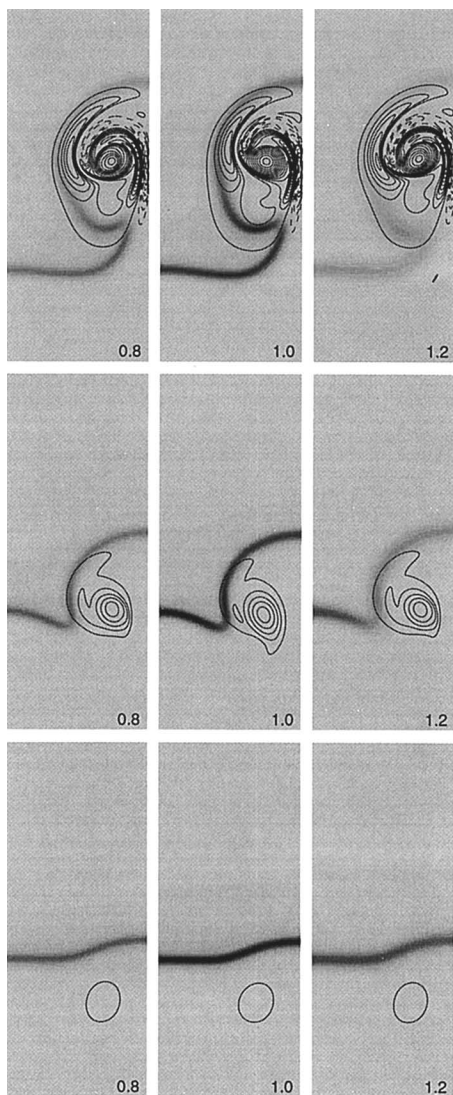


FIG. 1. Heat release rate (shading) and vorticity (contours) distributions at  $t = 0.5$  ms. Shown are results at lean (left), stoichiometric (center), and rich (right) conditions, for strong (top), intermediate (middle), and weak (bottom) vortices.

shows that, in each flow case, the rich flame responds significantly faster than either the lean or stoichiometric flames. In earlier work [15] we noted that for case F the heat release in the rich flame responds faster than in the stoichiometric flame, in contrast to earlier one-dimensional flame results [2]. The present computations enable us to amplify the previous finding, since the same observation holds even as the strain rate is varied (reduced) over a tenfold range. Remarkably, the present computations also indicate

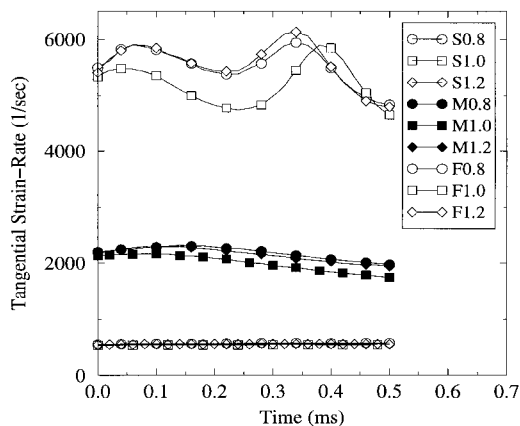


FIG. 2. Tangential strain rate time history at the flame  $10\% Y_{\text{fuel,max}}$  location on the vortex pair centerline. Curves correspond to the slow vortex pair at lean (S0.8), stoichiometric (S1.0) and rich conditions (S1.2); the intermediate vortex pair at lean (M0.8), stoichiometric (M1.0) and rich conditions (M1.2); and the fast vortex pair at lean (F0.8), stoichiometric (F1.0), and rich conditions (F1.2).

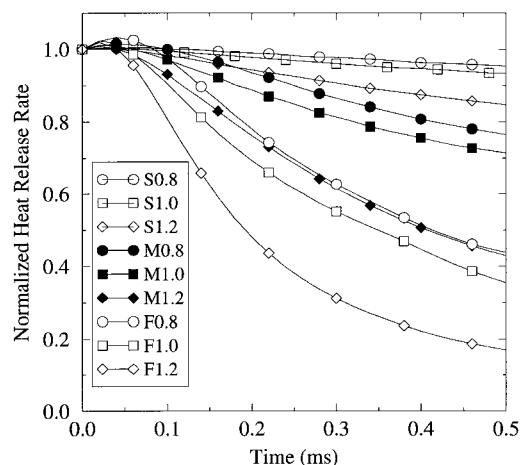


FIG. 3. Evolution of the normalized peak heat release rate on the vortex pair centerline. Curves are labeled as in Fig. 2.

that the lean flame, which is less robust than the stoichiometric flame, exhibits slower heat release decay rate than the latter. This observation also holds for all the flow speeds considered.

We have also suggested in Ref. [15] that the global flame response time is governed by the relative roles of H and OH in the kinetics and the faster response time of H versus OH. The lean and rich flames are both weak relative to the stoichiometric flame. At  $t = 0$ , peak heat release rates are 147, 306, and 176  $\text{cal/cm}^3 \cdot \text{s}$  for  $\Phi = 0.8, 1.0$ , and 1.2, respectively.

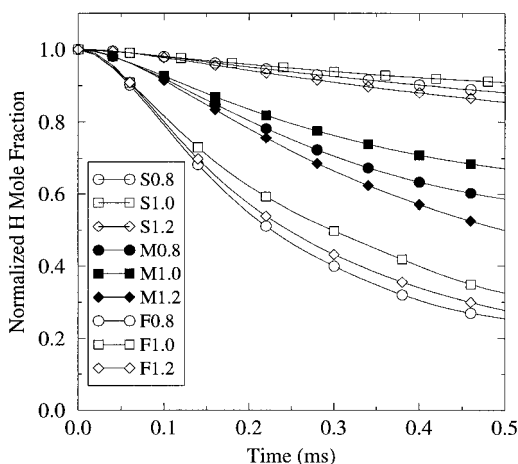


FIG. 4. Evolution of the normalized peak H mole fraction on the centerline of the vortex pair. Curves are labeled as in Fig. 2.

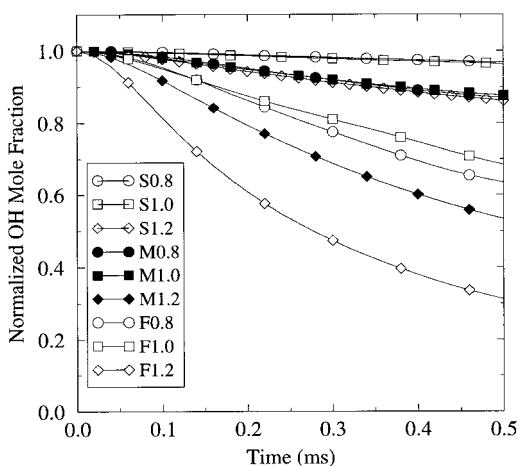


FIG. 5. Evolution of the normalized peak OH mole fraction on the centerline of the vortex pair. Curves are labeled as in Fig. 2.

Thus, robustness (e.g., peak fuel consumption or heat release rates) would not explain the trends in the figure. On the other hand, we find that for hydrocarbon species on the path to HCO (thus associated with primary heat release in the fuel consumption layer), for example,  $\text{CH}_4$ ,  $\text{CH}_2\text{O}$ , and HCO, the ratio of carbon flux carried by H reactions to that carried by OH reactions increases with  $\Phi$ . This suggests that the relative role of H versus OH in the fuel-consumption chemistry is significantly enhanced in going from lean to stoichiometric to rich, consistent with the change in response time of the heat release. Moreover, the ratio of available H to OH increases accordingly. Thus, since H has a

faster response than OH in this flame, the heat release rate responds at faster timescales as  $\Phi$  increases, due to the decreased role of OH and increased role of H. Also note that the pathway from  $\text{CH}_3$  to  $\text{CH}_2\text{O}$  relies primarily on O, rather than H and OH. On the other hand, we find the response of O to be as fast or faster than that of H in all cases, and so O does not appear to play a limiting role in the response of the heat release rate.

### OH and H

The response of H and OH, alluded to above, is illustrated in Figs. 4 and 5. The results show that the OH response rate approaches that of H only at  $\Phi = 1.2$ , but is still slower even then. The results also indicate that the response of H and OH have complex dependence on  $\Phi$  and  $\Gamma$ , which does *not* coincide with the response of the heat release rate. Specifically, while H mole fraction decays fastest at  $\Phi = 1.2$  in cases S and M, in case F it is the lean flame that exhibits fastest H decay. This indicates that interesting changes occur at large strain amplitudes.

It is also interesting to note that the stoichiometric flame has the slowest H decay rate, in contrast to the above observations for  $w_T$ . Meanwhile, Fig. 5 shows that at fixed  $\Gamma$ , OH decays fastest in the rich flame, in agreement with the heat release; this supports the observation that OH is a limiting factor in overall flame response. The lean and stoichiometric flames, on the other hand, have similar OH response in cases S and M, while the lean case is slightly faster in case F; this behavior is not consistent with that of the heat release rate.

### $\text{CH}_2\text{O}$ , HCO, and $[\text{OH}][\text{CH}_2\text{O}]$

The response of peak  $\text{CH}_2\text{O}$  (not shown) is similar to that of OH and exhibits similar dependence on  $\Phi$  and  $\Gamma$ . On the other hand, the response of peak HCO (also omitted) closely coincides with that of heat release rate (Fig. 3). This is in agreement with and extends the correlation established between HCO mole fraction and heat release rate in Refs. [11,23]. As outlined in Ref. [9], experimental challenges associated with measurement of HCO motivate the use of the peak concentration product of  $[\text{OH}][\text{CH}_2\text{O}]$  as surrogate. This product was in fact found to be an acceptable surrogate of both HCO and  $w_T$  in [9,23]. The same trend is observed in the present computations at all values of  $\Phi$  and  $\Gamma$ , which amplifies the scope of previous findings.

### $\text{CH}_3\text{O}$

The complexity of the flame response is also reflected in the evolution of the methoxy radical,  $\text{CH}_3\text{O}$ , shown in Fig. 6.  $\text{CH}_3\text{O}$  exhibits transient accumulation whose amplitude increases with  $\Gamma$ . For

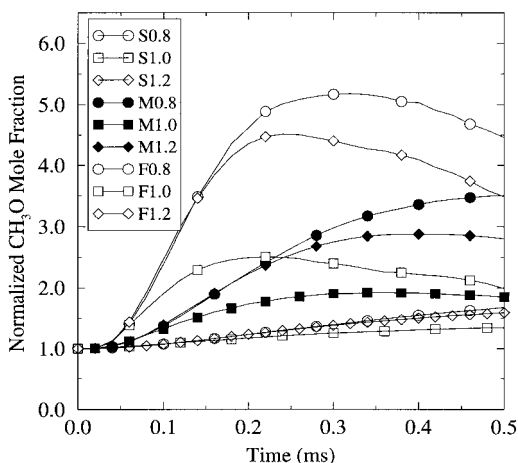


FIG. 6. Evolution of the normalized peak  $\text{CH}_3\text{O}$  mole fraction on the centerline of the vortex pair. Curves are labeled as in Fig. 2.

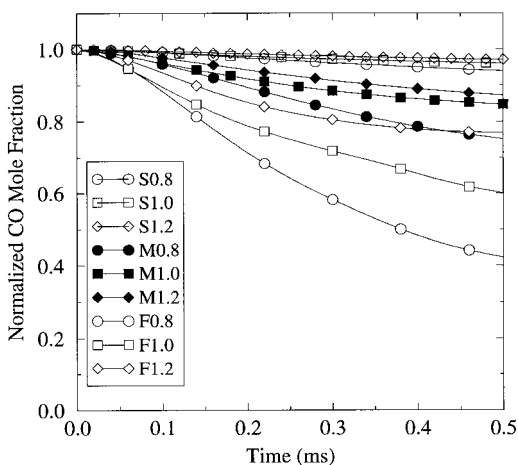


FIG. 7. Evolution of the normalized peak CO mole fraction on the centerline of the vortex pair. Curves are labeled as in Fig. 2.

the lean F case, a fivefold increase in peak  $\text{CH}_3\text{O}$  mole fraction is achieved even as the flame proceeds toward extinction. At fixed  $\Gamma$ , the methoxy mole fraction exhibits shorter rise times in the lean and rich cases than in the stoichiometric flame. On the other hand, it achieves highest amplitude of transient accumulation in the lean case, which has the smallest peak heat release rate. The more robust stoichiometric flame is the one having the smallest amplitudes and the longest rise times.

### CH

The peak CH mole fraction exhibits a similar dependence on  $\Phi$  and  $\Gamma$  as OH (Fig. 5); the results for

CH are therefore omitted. In particular, as for  $w_T$ , CH decay is fastest in the rich flame. The response of CH in the lean and stoichiometric cases is almost identical in cases S and M. On the other hand, as with OH, the lean case exhibits faster decay rate of peak CH in case F; this behavior is not in agreement with the trends established for  $w_T$ .

### CO

The response of peak CO is shown in Fig. 7, which indicates a monotonous *decrease* in speed of response with increasing  $\Phi$ . This behavior, which is observed at all values of  $\Gamma$ , is in contrast with the response of  $w_T$  (Fig. 3) and HCO. This is somewhat surprising, since HCO is the major source of CO. In fact, we do find that the response of the peak CO production rate increases with  $\Phi$  in a manner similar to HCO and  $w_T$ . This suggests that the cause of the inverse behavior of CO mole fraction is due to transport, rather than reaction. Inspection of CO mole fraction profiles reveals that the amount of CO behind the flame increases with  $\Phi$ , dictated by the corresponding increase in the equilibrium concentration of CO in the products. The absence of radiant heat losses in the model leads to a higher plateau of temperature and CO in the products region, as compared with a non-adiabatic flame model. Moreover, higher levels of CO are obtained at higher  $\Phi$ . This increase in the available CO behind the flame then leads to a reduction in the decay rate of peak CO mole fraction as  $\Phi$  increases. Even with radiant losses included, the products CO level in the immediate vicinity of the flame is expected to increase with  $\Phi$ , so the role of transport in the decay rate of CO may also be observed in a non-adiabatic setting. This is a subject for future work.

### Conclusions

A parametric study is conducted of the interaction of a premixed methane/air flame with a counter-rotating vortex pair under a range of reactants stoichiometry and flow time scales. Attention is focused on the transient response of the heat release and flame structure on the vortex pair centerline. In particular, computed results indicate the following.

1. For all values of  $\Gamma$  considered, the heat release timescale decreases as  $\Phi$  increases. This trend generalizes earlier findings in Ref. [15], which were restricted to fast vortices and to stoichiometric and rich conditions. Remarkably, and in contrast with results for one-dimensional flames under sinusoidal stretching, the slower propagating rich flame responds faster than the stoichiometric flame. Meanwhile, the lean flame responds at a slightly slower rate than the stoichiometric flame. Consequently, the response

time scale does *not* generally correlate with peak heat release rate or the fuel consumption rate.

2. The response of the heat release rate appears to be governed by the relative roles of H and OH in the kinetics. As  $\Phi$  increases, more of the fuel consumption pathways are dominated by H reactions due to the scarcity of OH and therefore respond at the faster H time scales.
3. At all values of  $\Phi$  and  $\Gamma$ , the peak HCO mole fraction exhibits a response similar to that of the peak heat release rate. By including a wide range of flow timescales as well as lean conditions, the present results extend the scope of earlier correlations [11,23].
4. The responses of H and OH exhibit some similarities with that of heat release rate but reveal differences which depend on  $\Gamma$ . Meanwhile, the response of  $\text{CH}_3\text{O}$  reveals transient accumulations with highest amplitude occurring in the lean flame. The decay of peak CO is fastest in the lean flame, in contrast with  $w_T$ , HCO, and the CO production rate. The results suggest that transport plays a dominant role in the observed CO behavior.

The observed dependence of the flame response on strain and stoichiometry does not appear to follow a simple correlation based on global parameters, such as heat release rate, propagation speed, or flame thickness. In particular, the computations indicate that the flame kinetics play a dominant role in the transient behavior of the heat release rate. This prevents us from adapting simplified interpretations based on diffusion timescales. Despite considering a wide range of flow timescales and varying the mixture stoichiometry, a sharp contrast exists between the present two-dimensional computations and earlier results for one-dimensional flames under sinusoidal forcing. The present experiences suggest that this discrepancy is unlikely to be due to the strain rate amplitudes. An extended investigation is currently being planned to further explore this issue.

#### Acknowledgment

This work was supported by the U.S. Department of Energy, Office of Basic Energy Sciences, Chemical Sciences Division. Computations were performed at the National Center for Supercomputer Applications.

#### REFERENCES

1. Ghoniem, A. F., Soteriou, M. C., Knio, O. M., and Cetegen, B., *Proc. Combust. Inst.* 24:223–230 (1992).
2. Egolfopoulos, F. N., *Proc. Combust. Inst.* 25:1365–1373 (1994).
3. Petrov, C. A., and Ghoniem, A. F., *Combust. Flame* 102:401–417 (1995).
4. Ashurst, W. T., and McMurtry, P. A., *Combust. Sci. Technol.* 66:17–37 (1989).
5. Rutland, C. J., and Ferziger, J. H., *Combust. Flame* 84:343–360 (1991).
6. Poinot, T., Veynante, D., and Candel, S., *J. Fluid Mech.* 228:561–606 (1991).
7. Samaniego, J.-M., and Mantel, T., *Combust. Flame*, 118:537–556 (1999).
8. Nguyen, Q.-V., and Paul, P. H., *Proc. Combust. Inst.* 26:357–364 (1996).
9. Paul, P. H., and Najm, H. N., *Proc. Combust. Inst.* 27:43–50 (1998).
10. Najm, H. N., and Wyckoff, P. S., *Combust. Flame* 110:92–112 (1997).
11. Najm, H. N., Paul, P. H., Mueller, C. J., and Wyckoff, P. S., *Combust. Flame* 113:312–332 (1998).
12. Roberts, W. L., Driscoll, J. F., Drake, M. C., and Goss, L. P., *Combust. Flame* 94:58–69 (1993).
13. Mueller, C. J., Driscoll, J. F., Sutkus, D. J., Roberts, W. L., Drake, M. C., and Smooke, M. D., *Combust. Flame* 100:323–331 (1995).
14. Mueller, C. J., Driscoll, J. F., Reuss, D. L., Drake, M. C., and Rosalik, M. E., *Combust. Flame* 112:342–358 (1998).
15. Najm, H. N., Knio, O. M., Paul, P. H., and Wyckoff, P. S., *Combust. Theory Modelling* 3:709–726 (1999).
16. Najm, H. N., Wyckoff, P. S., and Knio, O. M., *J. Comput. Phys.* 143:381–402 (1998).
17. Knio, O. M., Najm, H. N., and Wyckoff, P. S., *J. Comput. Phys.* 154:428–467 (1999).
18. Majda, A., and Sethian, J., *Combust. Sci. Technol.* 42:185–205 (1985).
19. Brown, P. N., Byrne, G. D., and Hindmarsh, A. C., *SIAM J. Sci. Stat. Comput.* 10:1038–1051 (1989).
20. Kee, R. J., Rupley, F. M., and Miller, J. A., Sandia report SAND89-8009B.
21. Kee, R. J., Grcar, J. F., Smooke, M. D., and Miller, J. A., Sandia report SAND85-8240.
22. Frenklach, M., Wang, H., Goldenberg, M., Smith, G. P., Golden, D. M., Bowman, C. T., Hanson, R. K., Gardiner, W. C., and Lissianski, V., report GRI-95/0058.
23. Najm, H. N., Knio, O. M., Paul, P. H., and Wyckoff, P. S., *Combust. Sci. Technol.* 140:369–403 (1998).